# Supplemental Material for Exchange-Correlation Functional Challenges in Modeling Quaternary Chalcogenides

Robert B. Wexler†, Gopalakrishnan Sai Gautam†, and Emily A. Carter†‡

*†Department of Mechanical and Aerospace Engineering, Princeton University, Princeton, NJ 08544-5263, United States and ‡ Office of the Chancellor and Department of Chemical and Biomolecular Engineering, University of California, Los Angeles, CA 90095, United States*

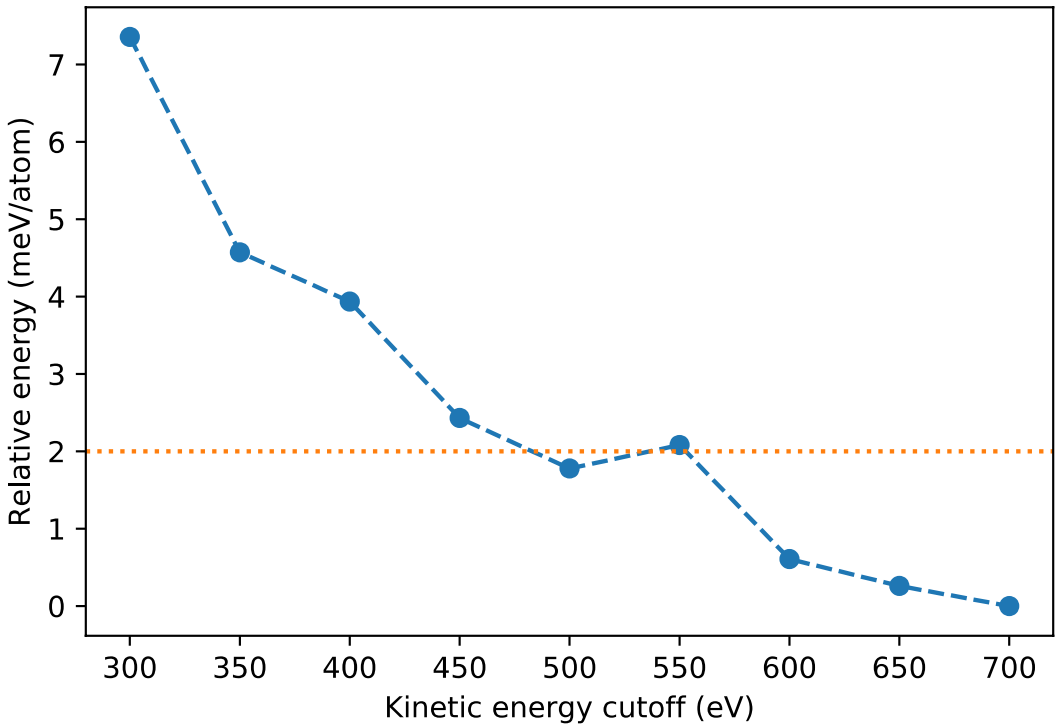


Figure S1. Planewave basis set convergence tests for SCAN calculations of $Cu_2ZnSnS_4$. A 500 eV kinetic energy cutoff is sufficient to obtain 2 meV/atom (dotted orange line) convergence of the total energy.

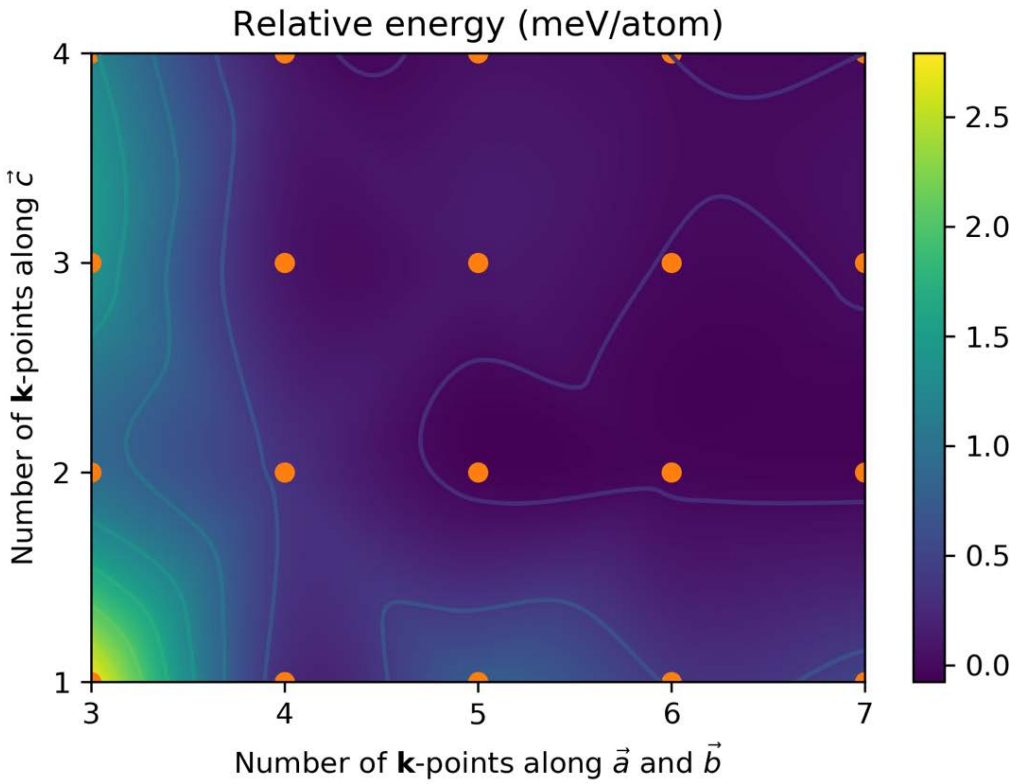


Figure S2. $\boldsymbol{k}$-point convergence tests for SCAN calculations of $Cu_2ZnSnS_4$. The relative energy is interpolated between data points (orange circles) using a cubic spline. A $6 \times 6 \times 3$, $\Gamma$-point-centered $\boldsymbol{k}$-point grid, which corresponds to the 8 $k$-points per 4 Å mentioned in the main text, is sufficient to obtain <0.5 meV/atom convergence of the total energy.

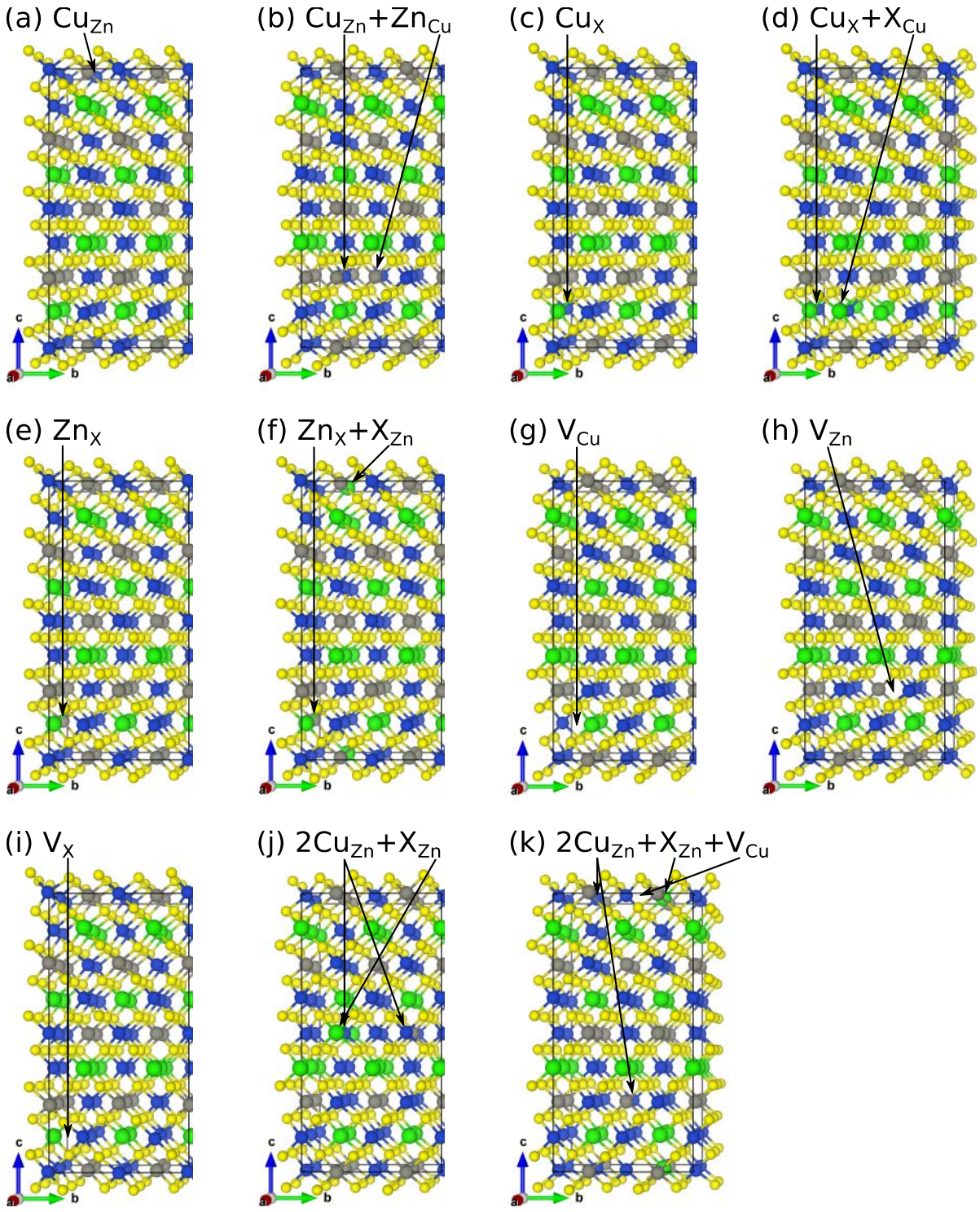


Figure S3. Defect configurations for $Cu_2ZnXS_4$ where X is either Sn or Ge. Blue, gray, green, and yellow balls correspond to Cu, Zn, X (Sn/Ge), and S, respectively. Arrows point to the locations of individual defects. Atoms in the top and bottom layers are the same. Defect configurations are taken from Ref. 1 and our unpublished work. Placement of these defects is decided by generating all unique defect configurations, calculating their SCAN total energies, and finding the minimum energy structure.

(A) Stannite ($I42m$, 121)

(B) Wurzite ($Pmn2_1$, 31)

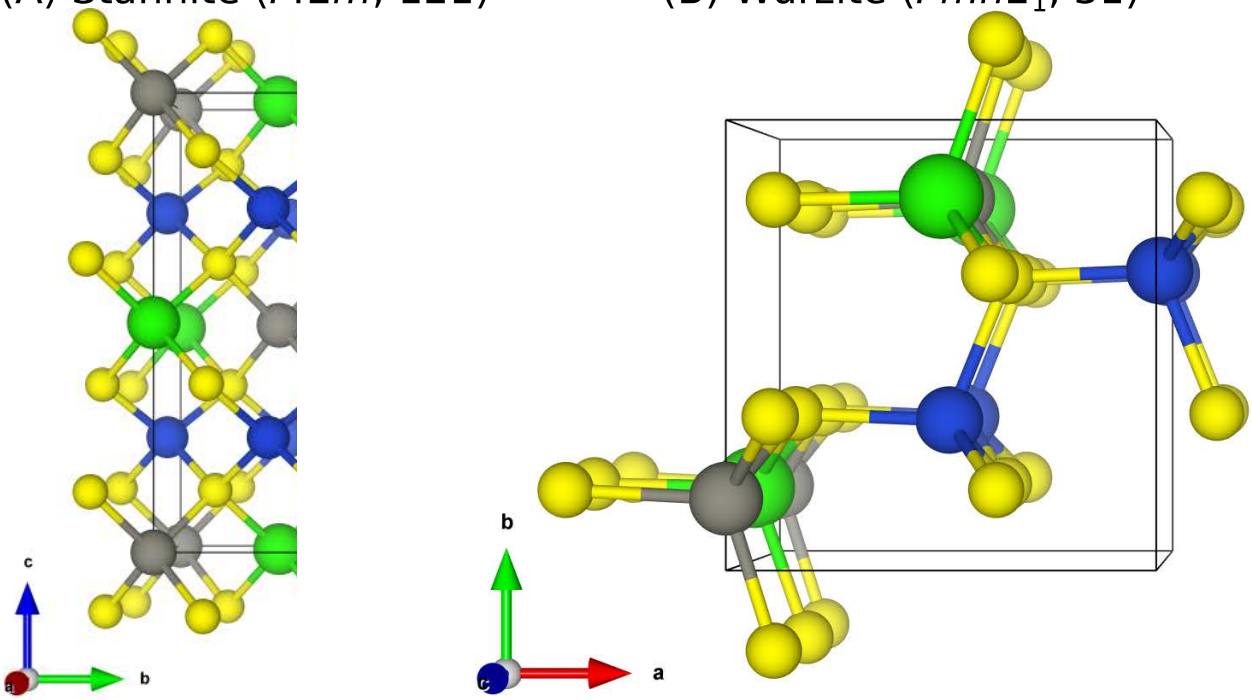


Figure S4. Crystal structures of stannite and wurtzite $Cu_2ZnXS_4$ where X is either Sn or Ge. Blue, gray, green, and yellow balls correspond to Cu, Zn, X (Sn/Ge), and S, respectively.

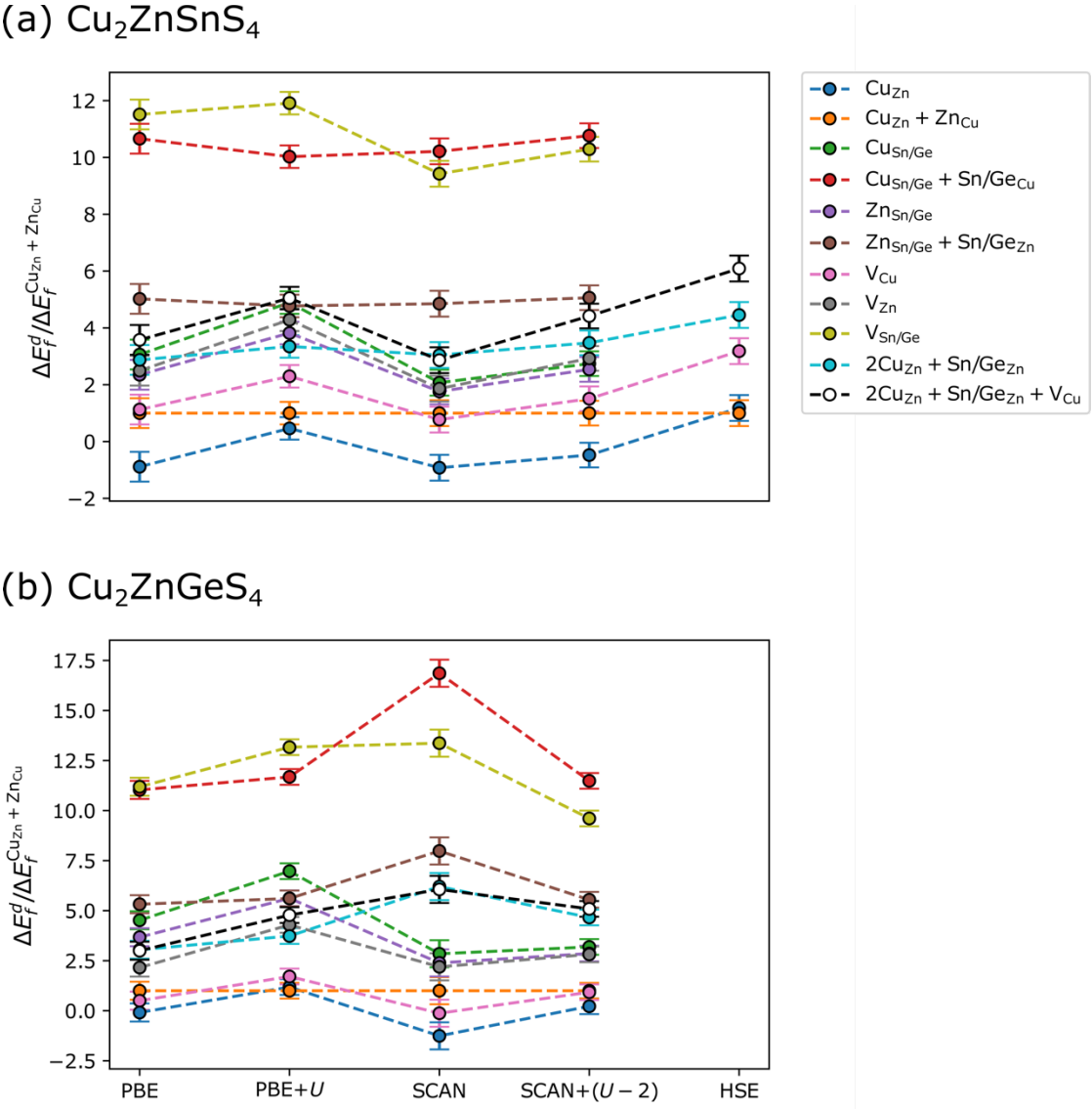


Figure S5. XC functional dependence of qualitative defect formation energy ($\Delta E_f^d$) trends in (a) $Cu_2ZnSnS_4$ and (b) $Cu_2ZnGeS_4$. The vertical axis corresponds to the $\Delta E_f^d$ relative to that of $Cu_{Zn}$+$Zn_{Cu}$, i.e., the defect with the best agreement between XC functionals. Error bars indicate that the formation energies are converged to within 0.1 eV (see Table S6), which is within usual convergence bounds employed for defect calculations in periodic boundary conditions.[2–4] The intersection of two dashed lines indicates a qualitative disagreement between XC functionals in the stability order of defects. (a) and (b) show generally strong agreement between XC functionals with the following exceptions. For both $Cu_2ZnSnS_4$ and $Cu_2ZnGeS_4$, $Cu_{Sn/Ge}$ (dashed green line) and $2Cu_{Zn}$+$Sn/Ge_{Zn}$ (cyan) intersect, leading to a significant change in their relative stability order where we define a significant intersection/change as one in which the $\Delta E_f^d$, in their pre- and post-intersection stability order, differ by more than 0.1 eV. For $Cu_2ZnSnS_4$, $V_{Zn}$ (gray) and $2Cu_{Zn}$+$Sn_{Zn}$ (cyan) intersect significantly. For $Cu_2ZnGeS_4$, (1) $Zn_{Ge}$ (purple) intersects with $2Cu_{Zn}$+$Ge_{Zn}$ (cyan) and $2Cu_{Zn}$+$Ge_{Zn}$+$V_{Cu}$ (white), (2) $Cu_{Ge}$ (green) also intersects with $2Cu_{Zn}$+$Ge_{Zn}$ (cyan) and $Zn_{Ge}$+$Ge_{Zn}$ (brown), and (3) $Cu_{Ge}$+$Ge_{Cu}$ (red) intersects with $V_{Ge}$ (yellow).

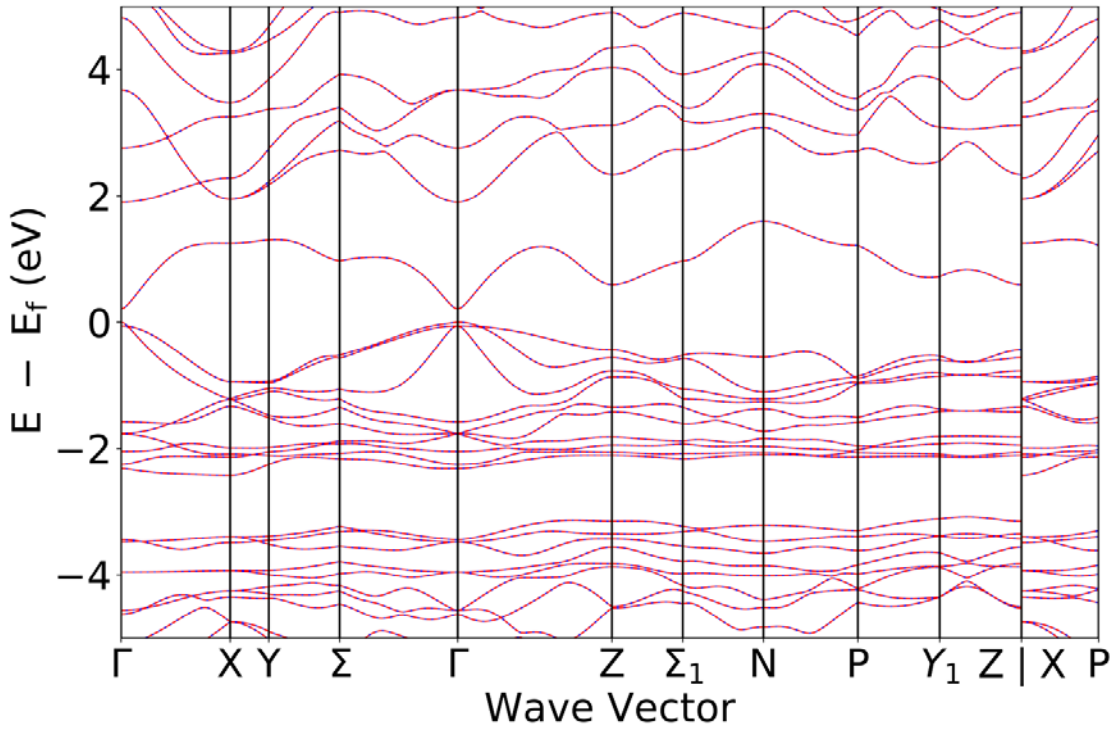


Figure S6. DFT-PBE band structure of CZTS, which has a direct band gap of 0.21 eV at the Γ-point. The high-symmetry *k*-path was generated using the approach discussed in Ref. 5. Band structures were plotted using pymatgen.[6]

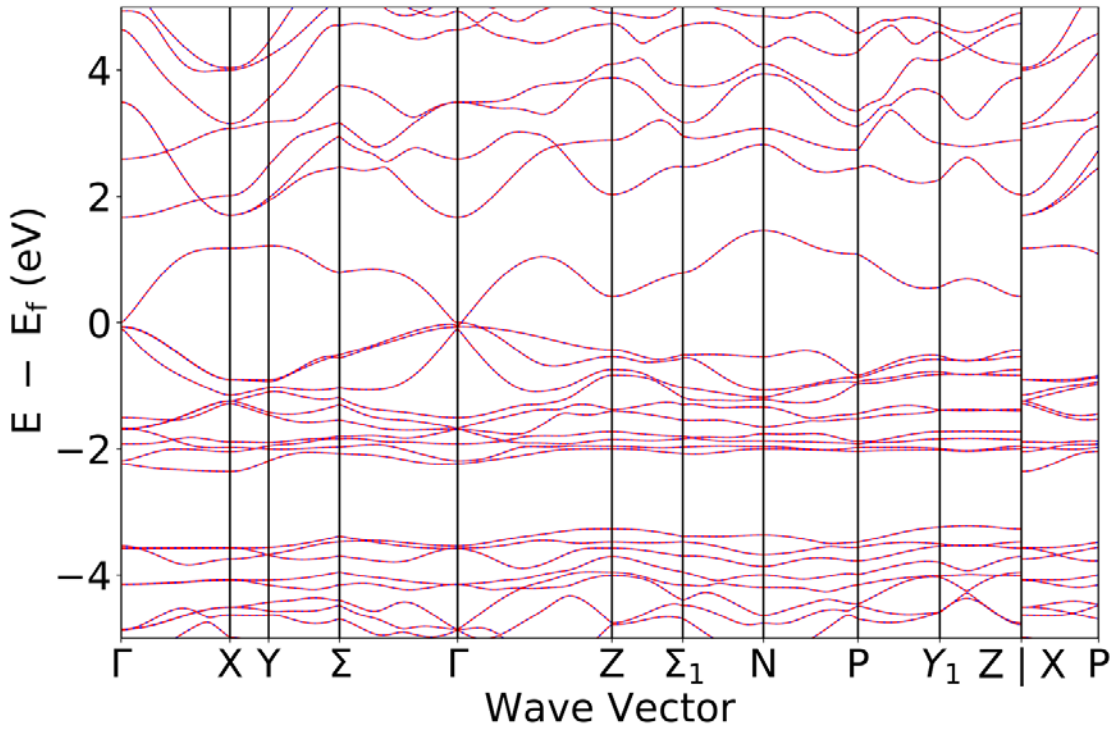


Figure S7. DFT-SCAN band structure of CZTS, which has a direct band gap of 0.02 eV at the Γ-point.

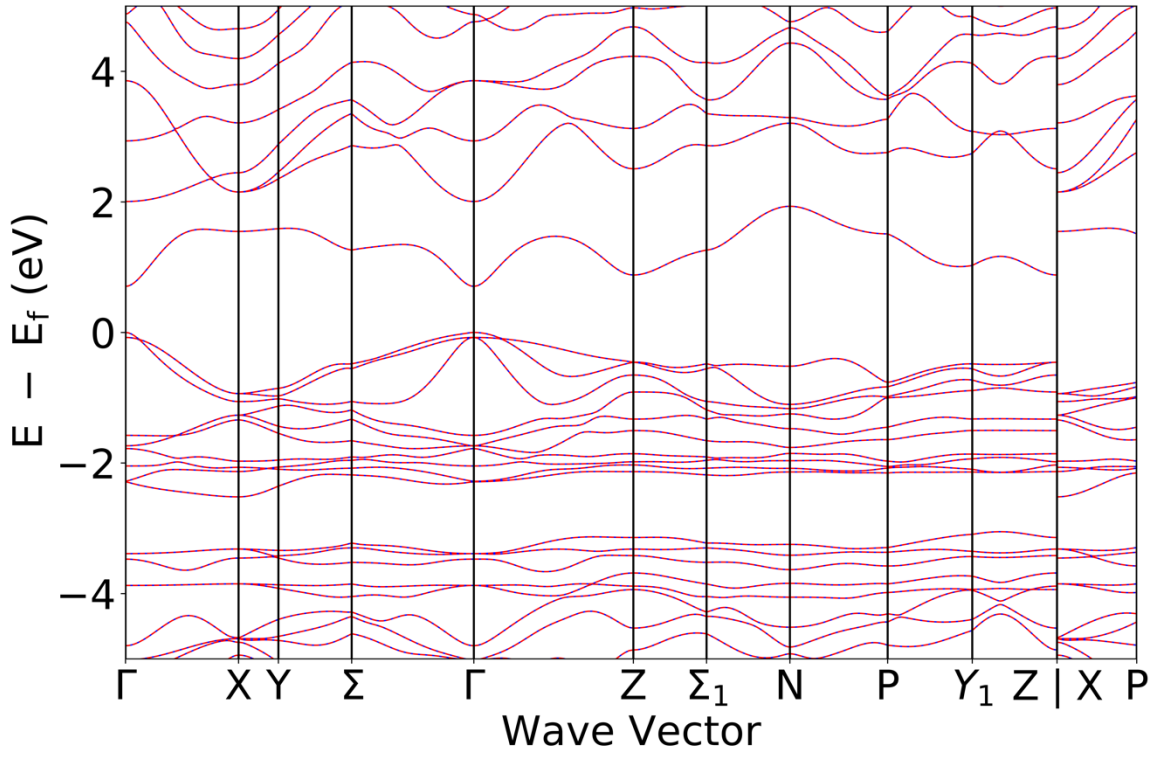


Figure S8. DFT-PBE band structure of CZGS, which has a direct band gap of 0.71 eV at the Γ-point.

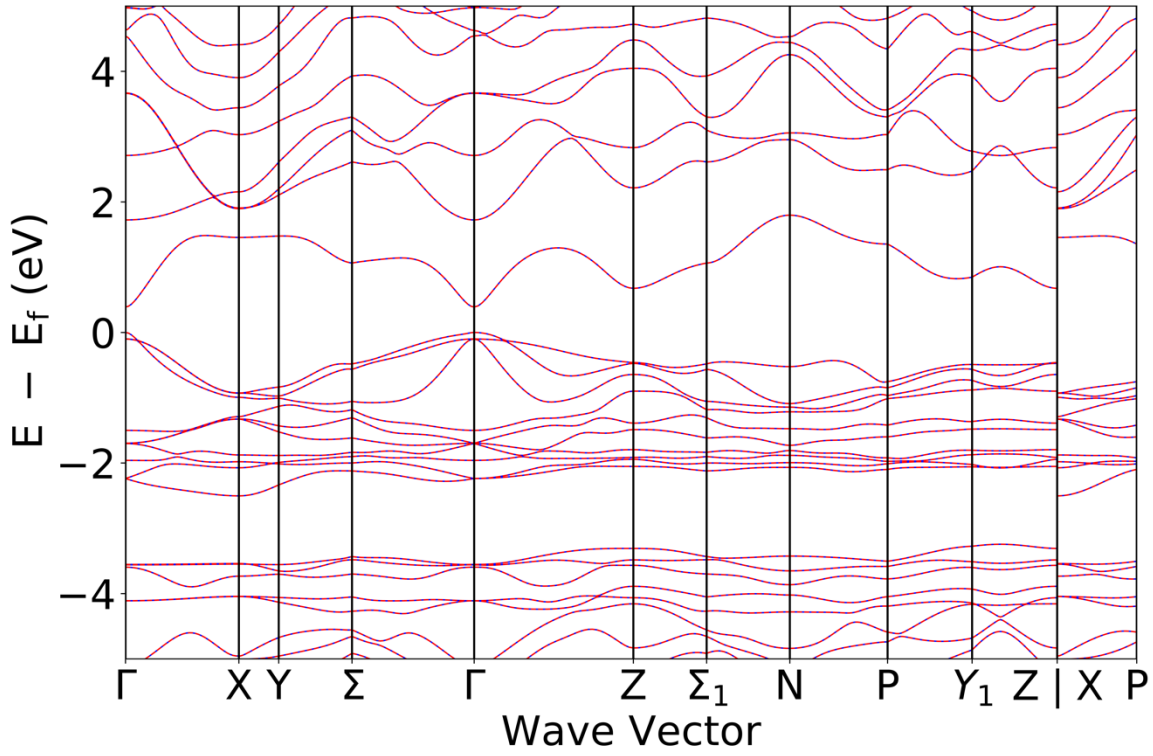


Figure S9. DFT-SCAN band structure of CZGS, which has a direct band gap of 0.39 eV at the Γ-point.

Table S1. Effect of Ge semicore 3d states on SCAN 0 K formation energies ($\Delta E_f^{0K}$) of Ge-containing compounds. $Without\ 3d$ and $With\ 3d$ correspond to relaxations (where ionic positions, cell volume, and cell shape are allowed to change) using the $4s^2\ 4p^2$ and $4s^2\ 3d^{10}\ 4p^2$ PAW data sets for Ge, respectively. The inclusion of semicore 3d states in the PAW data set for Ge only marginally affects the $\Delta E_f^{0K}$ of compounds containing Cu, Ge, S, Sn, and Zn.

| **Compound** | $\boldsymbol{\Delta E_f^{0K}}$ **(eV/atom)** | | $\boldsymbol{With\ 3d - Without\ 3d}$ **(meV/atom)** |
|---|---|---|---|
| | $\boldsymbol{Without\ 3d}$ | $\boldsymbol{With\ 3d}$ | |
| $Cu_3Ge$ | -0.05 | -0.05 | -3.90 |
| GeS | -0.25 | -0.25 | 1.38 |
| $GeS_2$ | -0.36 | -0.37 | -4.01 |
| $Cu_2GeS_3$ | -0.39 | -0.39 | -0.44 |
| $Cu_4GeS_4$ | -0.31 | -0.31 | -0.03 |
| $Cu_8GeS_6$ | -0.23 | -0.23 | -1.85 |
| $SnGeS_3$ | -0.40 | -0.40 | -2.96 |
| $Cu_2ZnGeS_4$ | -0.54 | -0.54 | -0.31 |

Table S2. Effect of Cu semicore 3p states on $\Delta E_f^{0K}$ of Cu-containing compounds, the SCAN 0 K kesterite to stannite reaction energy ($\Delta E_{rxn}^{0K}$) for $Cu_2ZnSnS_4$, and SCAN 0 K Cu chemical potentials ($\mu_{Cu}$) for the Cu-poor and constrained Cu-poor conditions. The $\mu_{Cu}$ are referenced to the SCAN energy of pure Cu in its ground-state structure at 0 K, i.e., $Fm\bar{3}m$ (225). $Without\ 3p$ and $With\ 3p$ correspond to relaxations (where ionic positions, cell volume, and cell shape are allowed to change) using the $4s^1\ 5d^{10}$ and $3p^6\ 4s^1\ 5d^{10}$ PAW data sets for Cu, respectively. The inclusion of semicore 3p states in the PAW data set for Cu only marginally affects the $\Delta E_f^{0K}$ of compounds containing Cu (i.e., $Cu_2S$, $Cu_7S_4$, CuS, $CuS_2$, and both kesterite and stannite $Cu_2ZnSnS_4$), $\Delta E_{rxn}^{0K}$, or $\mu_{Cu}$ for the Cu-poor and constrained Cu-poor conditions.

| **Compound** | $\boldsymbol{\Delta E_f^{0K}}$ **(eV/atom)** | | $\boldsymbol{With\ 3p - Without\ 3p}$ **(meV/atom)** |
|---|---|---|---|
| | $\boldsymbol{Without\ 3p}$ | $\boldsymbol{With\ 3p}$ | |
| $Cu_2S$ | -0.19 | -0.18 | 15.44 |
| $Cu_7S_4$ | -0.23 | -0.21 | 12.08 |
| CuS | -0.27 | -0.27 | 9.03 |
| $CuS_2$ | -0.17 | -0.17 | 6.39 |
| $Cu_2ZnSnS_4$ (kesterite) | -0.54 | -0.53 | 6.17 |
| $Cu_2ZnSnS_4$ (stannite) | -0.53 | -0.53 | 5.89 |

| **Reaction** | $\boldsymbol{\Delta E_{rxn}^{0K}}$ **(eV/formula unit)** | | $\boldsymbol{With\ 3p - Without\ 3p}$ **(meV/atom)** |
|---|---|---|---|
| | $\boldsymbol{Without\ 3p}$ | $\boldsymbol{With\ 3p}$ | |
| $Kesterite \rightarrow Stannite$ | 0.06 | 0.05 | -0.28 |

| **Chemical potential condition** | $\boldsymbol{\mu_{Cu}}$ **(eV/atom)** | | $\boldsymbol{With\ 3p - Without\ 3p}$ **(meV/atom)** |
|---|---|---|---|
| | $\boldsymbol{Without\ 3p}$ | $\boldsymbol{With\ 3p}$ | |
| Cu-poor | -0.57 | -0.54 | 24.69 |
| Constrained Cu-poor | -0.38 | -0.35 | 24.69 |

Table S3. SCAN $\Delta E_f^{0K}$ and experimental 298 K formation enthalpies ($\Delta H_f^{298K}$). Space groups are given by their international short symbol and number (in parentheses). All structures are optimized at the level of DFT-SCAN. Incorrect phase assignments are highlighted in yellow. †SCAN+rVV10 corrects phase assignment but not the magnitude of $\Delta E_f^{0K}$. ‡Correct phase, i.e., $C2/c$ (15), is 4 meV/atom higher in energy. We select the $\Delta H_f^{Exp}$ of Figure 2 in the main text from those of Refs. 7–13. Ref. 7 is used by the Materials Project[14] and, therefore, is our preferred source of experimental thermochemical data. We apply the following rules in order to select the $\Delta H_f^{Exp}$: (1) if a compound has one $\Delta H_f^{298K}$, then set its $\Delta H_f^{Exp} = \Delta H_f^{298K}$; (2) if a compound has two $\Delta H_f^{298K}$, then set its $\Delta H_f^{Exp} = \Delta H_f^{298K}[Ref.\ \min(n)]$ where $n$ is the Ref. number (e.g., for $GeI_2$, since $n = \{4, 5\}$, $\min(n) = 4$ and $\Delta H_f^{Exp} = \Delta H_f^{298K}[Ref.\ 4]$); (3) if a compound has three or more $\Delta H_f^{298K}$, then set its $\Delta H_f^{Exp}$ equal to the mode of $\{\Delta H_f^{298K}\}$ (i.e., the $\Delta H_f^{298K}$ that appears most often); and (4) if $\{\Delta H_f^{298K}\}$ has two or more modes, then set its $\Delta H_f^{Exp} = \Delta H_f^{298K}[Ref.\ \min(n)]$.

| **Compound** | **Space group**[15] | $\Delta E_f^{0K}$ | $\Delta H_f^{298K}$ (eV/atom) | | | | | |
|---|---|---|---|---|---|---|---|---|
| | | **(eV/atom)** | **Ref. 7** | **Ref. 8** | **Ref. 9** | **Ref. 10** | **Ref. 11** | **Other** |
| $Cu_3Ge$ | $Pmmn$ (59) | -0.05 | | | | | | -0.04[12] |
| GeS | $Pnma$ (62) | -0.25 | -0.39 | -0.39 | -0.36 | -0.32 | -0.39 | |
| $GeS_2$ | $P2_1/c$ (14)† | -0.37 | -0.54 | -0.54 | -0.65 | -0.42 | | |
| $Ge_3N_4$ | $P31c$ (159) | -0.18 | -0.10 | | -0.09 | -0.59 | | |
| $GeF_2$ | $P2_12_12_1$ (19) | -2.18 | -2.27 | | | -2.27 | | |
| $GeO_2$ | $P4_2/mnm$ (136) | -1.87 | -2.00 | -2.00 | -1.90 | -2.00 | 0.15 | |
| GeP | $C2/m$ (12) | -0.01 | -0.14 | -0.11 | -0.11 | -0.11 | | |
| $Cu_2GeS_3$ | $Cc$ (9) | -0.39 | | | | | | |
| $Cu_4GeS_4$ | $P2_1/c$ (14) | -0.31 | | | | | | |
| $Cu_8GeS_6$ | $Pmn2_1$ (31) | -0.23 | | | | | | |
| $SnGeS_3$ | $P2_1/c$ (14) | -0.40 | | | | | | |
| $Cu_2ZnGeS_4$ | $I\bar{4}$ (82) | -0.54 | | | | | | |
| $GeI_2$ | $P\bar{3}m1$ (164) | -0.31 | | | -0.30 | -0.27 | | |
| $GeI_4$ | $Pa\bar{3}$ (205) | -0.27 | -0.08 | | -0.29 | -0.31 | | |
| GeSe | $Pnma$ (62) | -0.19 | -0.36 | -0.36 | -0.48 | -0.36 | -0.36 | |
| $GeSe_2$ | $P2_1/c$ (14) | -0.28 | -0.39 | -0.39 | | -0.39 | -0.39 | |
| GeTe | $R3m$ (160) | -0.04 | -0.17 | -0.25 | -0.13 | -0.25 | -0.25 | |
| $Mg_2Ge$ | $Fm\bar{3}m$ (225) | -0.30 | -0.40 | -0.36 | -0.38 | | | |
| $MgGeO_3$ | $R\bar{3}$ (148)‡ | -2.41 | | | | -2.52 | | |
| $Ni_2Ge$ | $Pnma$ (62) | -0.32 | -0.38 | -0.38 | | | | |
| SnS | $Pnma$ (62) | -0.45 | -0.37 | -0.45 | -0.34 | -0.22 | -0.22 | |
| $SnS_2$ | $P\bar{3}m1$ (164) | -0.42 | -0.53 | -0.62 | | -0.32 | -0.32 | |
| $Cu_2S$ | $P2_1/c$ (14) | -0.19 | -0.27 | -0.28 | -0.27 | -0.27 | | |
| CuS | $P6_3/mmc$ (194) | -0.27 | -0.27 | -0.28 | -0.28 | -0.29 | | |
| $Cu_2SnS_3$ | $C1c1$ (9) | -0.39 | | | | | | |

| Compound | Space group | $\Delta E_f^{0K}$ (eV/atom) | $\Delta H_f^{298K}$ (eV/atom) | | | | | |
|---|---|---|---|---|---|---|---|---|
| | | | Ref. 7 | Ref. 8 | Ref. 9 | Ref. 10 | Ref. 11 | Other |
| $Cu_4SnS_4$ | $Pnma$ (62) | -0.30 | | | | | | |
| $Cu_7S_4$ | $Pnma$ (62) | -0.23 | | | | | | -0.07[13] |
| $CuS_2$ | $P\bar{a}3$ (205) | -0.17 | | | | | | |
| $Sn_2S_3$ | $Pnma$ (62) | -0.43 | -0.55 | -0.55 | | -0.55 | -0.55 | |
| $Cu_2ZnSnS_4$ | $I\bar{4}$ (82) | -0.54 | | | | | | |
| ZnS | $F\bar{4}3m$ (216) | -0.94 | -1.06 | -1.06 | -1.07 | -1.05 | | |

Table S4. Polymorph preference in $Cu_2ZnSnS_4$ and $Cu_2ZnGeS_4$ does not depend on the XC functional.

| XC | $E_{stannite} - E_{kesterite}$ (eV/formula unit) | $E_{wurtzite} - E_{kesterite}$ (eV/formula unit) |
|---|---|---|
| | *$Cu_2ZnSnS_4$* | |
| PBE | 0.02 | 0.06 |
| PBE+$U$ | 0.03 | 0.05 |
| SCAN | 0.03 | 0.07 |
| SCAN+rVV10 | 0.03 | 0.07 |
| SCAN+$(U-2)$ | 0.03 | 0.06 |
| | *$Cu_2ZnGeS_4$* | |
| PBE | 0.04 | 0.04 |
| PBE+$U$ | 0.05 | 0.04 |
| SCAN | 0.04 | 0.05 |
| SCAN+rVV10 | 0.04 | 0.05 |
| SCAN+$(U-2)$ | 0.05 | 0.05 |

Table S5. SCAN+rVV10 does not affect strongly the formation energies of defects with varying numbers of holes generated. For $Cu_{Zn}$+$Zn_{Cu}$ and $V_{Sn}$ in CZTS and $Cu_{Zn}$+$Zn_{Cu}$ in CZGS, the difference between the SCAN and SCAN+rVV10 defect formation energies is within the error associated with using a $2 \times 2 \times 2$ supercell (Table S4) and, therefore, cannot be viewed as a significant deviation between the two methods. For $V_{Ge}$, the difference is 0.15 eV, which is significant but does not affect any qualitative trends.

| Compound | Defect | Number of holes generated | Defect formation energy (eV) | |
|---|---|---|---|---|
| | | | SCAN | SCAN+rVV10 |
| CZTS | $Cu_{Zn}$+$Zn_{Cu}$ | 0 | 0.22 | 0.20 |
| CZTS | $V_{Sn}$ | 4 | 2.07 | 2.05 |
| CZGS | $Cu_{Zn}$+$Zn_{Cu}$ | 0 | 0.15 | 0.25 |
| CZGS | $V_{Ge}$ | 4 | 1.97 | 2.12 |

Table S6. Convergence of the SCAN $2Cu_{Zn}+Sn_{Zn}+V_{Cu}$ formation energy with respect to supercell size. $n$ corresponds to the number of periodic repeats along the $a$, $b$, and $c$ crystallographic axes. A $2 \times 2 \times 2$ supercell is sufficient to obtain 0.1 eV convergence of the $2Cu_{Zn}+Sn_{Zn}+V_{Cu}$ formation energy. We analyze the effect of supercell size on the formation energy for $2Cu_{Zn}+Sn_{Zn}+V_{Cu}$ as it is the largest defect cluster we consider and is charge imbalanced, both of which increase the likelihood of interactions between periodic images.

| $n_a$ | $n_b$ | $n_c$ | Relative energy (eV) |
|---|---|---|---|
| 2 | 2 | 2 | -0.05 |
| 3 | 2 | 2 | -0.01 |
| 3 | 3 | 2 | 0.09 |
| 3 | 3 | 3 | 0.00 |

Table S7. XC functional dependence of unreferenced (i.e., not referenced to the energies of pure elements in their ground-state structures) chemical potentials ($\mu^{unref.}$) under Cu-poor conditions for CZTS and CZGS. The Cu-poor conditions are defined in the main text. Note that here we have subtracted 0.27 eV/Ge from SCAN+$(U-2)$ and SCAN+$U$ $\mu_{Ge}$ in accordance with the Ge correction described in the main text.

| XC | $\mu^{unref.}$ (eV/atom) | | | |
|---|---|---|---|---|
| | Cu | Zn | Sn/Ge | S |
| *CZTS* | | | | |
| PBE | -4.64 | -3.06 | -5.50 | -4.21 |
| PBE+$U$ | -3.49 | -2.77 | -6.09 | -4.21 |
| SCAN | -15.69 | -15.36 | -37.16 | -9.64 |
| SCAN+rVV10 | -15.48 | -15.12 | -36.95 | -9.54 |
| SCAN+$(U-2)$ | -15.15 | -15.19 | -37.49 | -9.64 |
| SCAN+$U$ | -14.55 | -15.10 | -37.82 | -9.64 |
| HSE | -4.37 | -3.16 | -5.84 | -5.23 |
| *CZGS* | | | | |
| PBE | -4.76 | -3.06 | -5.81 | -4.21 |
| PBE+$U$ | -3.65 | -2.77 | -6.38 | -4.21 |
| SCAN | -15.79 | -15.36 | -20.43 | -9.64 |
| SCAN+$(U-2)$ | -15.28 | -15.19 | -20.75 | -9.64 |
| HSE | -4.16 | -2.74 | -4.99 | -5.65 |

## Sample SCAN calculation of the Cu-poor condition for CZGS

In the Cu-poor condition, $Cu_2ZnGeS_4$ is in equilibrium with $GeS_2$, S, and ZnS. To determine the $\mu$ of Cu, Zn, S, and Ge for this condition, we solve the following set of equations

$$2\mu_{Cu} + \mu_{Zn} + \mu_{Ge} + 4\mu_S = E^{SCAN}_{Cu_2ZnGeS_4} - 0.27 \quad \text{(S1)}$$

$$\mu_{Ge} + 2\mu_S = E^{SCAN}_{GeS_2} - 0.27 \quad \text{(S2)}$$

$$\mu_S = E^{SCAN}_S \quad \text{(S3)}$$

$$\mu_{Zn} + \mu_S = E^{SCAN}_{ZnS} \quad \text{(S4)}$$

or the matrix equation

$$\begin{bmatrix} 2 & 1 & 1 & 4 \\ 0 & 0 & 1 & 2 \\ 0 & 0 & 0 & 1 \\ 0 & 1 & 0 & 1 \end{bmatrix} \begin{bmatrix} \mu_{Cu} \\ \mu_{Zn} \\ \mu_{Ge} \\ \mu_S \end{bmatrix} = \begin{bmatrix} E^{SCAN}_{Cu_2ZnGeS_4} - 0.27 \\ E^{SCAN}_{GeS_2} - 0.27 \\ E^{SCAN}_S \\ E^{SCAN}_{ZnS} \end{bmatrix} \quad \text{(S5)}$$

where the $E^{SCAN}$ is the SCAN total energy in eV/formula unit and the 0.27 eV/Ge subtracted from $E^{SCAN}_{Cu_2ZnGeS_4}$ and $E^{SCAN}_{GeS_2}$ is the Ge correction from the main text. The solution to Equation S5 is highlighted green in Table S7.

Table S8. Theoretical vs. experimental lattice constants of compounds containing Ge or in equilibrium with $Cu_2ZnSnS_4$ and $Cu_2ZnGeS_4$ under Cu-poor or constrained Cu-poor synthesis conditions (i.e., S, SnS, $SnS_2$, and ZnS) calculated using different XC functionals. There is only one set of theoretical values (SCAN) for $Cu_3Ge$, GeS, $GeS_2$, $Cu_2GeS_3$, $Cu_4GeS_4$, $Cu_8GeS_6$, and $SnGeS_3$ because these compounds are unstable under Cu-poor conditions and, therefore, were not included in the PBE, PBE+$U$, SCAN+$(U-2)$, and SCAN+$U$ convex hull constructions.

| **Compound** | **Lattice constants** Å **for $a$, $b$, and $c$** **deg for $\alpha$, $\beta$, and $\gamma$** | ***Exp*** **Ref. 15** | **PBE** | **PBE+$U$** | **SCAN** | **SCAN+ $(U-2)$** | **SCAN+$U$** |
|---|---|---|---|---|---|---|---|
| $Cu_3Ge$ | $a$ | 4.19 | | | 4.17 | | |
| | $b$ | 4.53 | | | 4.46 | | |
| | $c$ | 5.25 | | | 5.24 | | |
| | $\alpha=\beta=\gamma$ | 90.00 | | | 90.00 | | |
| GeS | $a$ | 3.65 | | | 3.61 | | |
| | $b$ | 4.31 | | | 4.48 | | |
| | $c$ | 10.45 | | | 10.67 | | |
| | $\alpha=\beta=\gamma$ | 90.00 | | | 90.00 | | |
| $GeS_2$ | $a$ | 6.67 | | | 6.76 | | |
| | $b$ | 11.46 | | | 11.80 | | |
| | $c$ | 16.12 | | | 16.20 | | |
| | $\alpha=\beta$ | 90.00 | | | 90.00 | | |
| | $\gamma$ | 90.00 | | | 90.72 | | |
| $Cu_2GeS_3$ | $a$ | 6.42 | | | 6.44 | | |
| | $b$ | 6.44 | | | 6.40 | | |
| | $c$ | 6.50 | | | 6.44 | | |
| | $\alpha$ | 60.33 | | | 60.24 | | |
| | $\beta$ | 81.04 | | | 80.65 | | |
| | $\gamma$ | 71.65 | | | 70.89 | | |
| $Cu_4GeS_4$ | $a$ | 9.80 | | | 9.71 | | |
| | $b$ | 9.96 | | | 9.93 | | |
| | $c$ | 13.22 | | | 13.09 | | |
| | $\alpha=\beta$ | 90.00 | | | 90.00 | | |
| | $\gamma$ | 100.97 | | | 100.84 | | |
| $Cu_8GeS_6$ | $a$ | 6.96 | | | 6.90 | | |
| | $b$ | 7.04 | | | 7.00 | | |
| | $c$ | 9.86 | | | 9.68 | | |
| | $\alpha=\beta=\gamma$ | 90.00 | | | 90.00 | | |
| $SnGeS_3$ | $a$ | 7.27 | | | 7.43 | | |
| | $b$ | 10.22 | | | 10.23 | | |
| | $c$ | 6.87 | | | 6.86 | | |
| | $\alpha=\gamma$ | 90.00 | | | 90.00 | | |
| | $\beta$ | 105.45 | | | 105.32 | | |

| Compound | Lattice constants Å for $a$, $b$, and $c$ deg for $\alpha$, $\beta$, and $\gamma$ | $Exp$ Ref. 15 | PBE | PBE+$U$ | SCAN | SCAN+ $(U-2)$ | SCAN+$U$ |
|---|---|---|---|---|---|---|---|
| $Cu_2ZnGeS_4$ | $a=b$ | 5.35 | 5.27 | 5.25 | 5.29 | 5.27 | 5.35 |
| | $c$ | 10.52 | 10.51 | 10.39 | 10.50 | 10.49 | 10.52 |
| | $\alpha$ | 90.00 | 90.00 | 89.96 | 89.94 | 90.00 | 90.00 |
| | $\beta$ | 90.00 | 90.00 | 89.98 | 89.96 | 90.00 | 90.00 |
| | $\gamma$ | 90.00 | 90.00 | 89.98 | 89.99 | 90.00 | 90.00 |
| $Cu_2ZnSnS_4$ | $a=b$ | 5.44 | 5.38 | 5.34 | 5.40 | 5.38 | 5.37 |
| | $c$ | 10.84 | 10.75 | 10.67 | 10.82 | 10.75 | 10.72 |
| | $\alpha=\beta=\gamma$ | 90.00 | 90.00 | 90.00 | 90.00 | 90.00 | 90.00 |
| S | $a$ | 10.17 | 10.57 | | 10.54 | | |
| | $b$ | 11.51 | 13.02 | | 12.94 | | |
| | $c$ | 23.53 | 24.74 | | 24.60 | | |
| | $\alpha=\gamma$ | 90.00 | 90.00 | | 90.00 | | |
| | $\beta$ | 90.00 | 90.00 | | 90.01 | | |
| SnS | $a$ | 11.20 | 11.35 | 11.18 | 11.31 | 11.19 | 10.97 |
| | $b$ | 3.98 | 3.98 | 3.94 | 3.95 | 3.91 | 3.89 |
| | $c$ | 4.32 | 4.36 | 4.27 | 4.50 | 4.49 | 4.50 |
| | $\alpha=\beta=\gamma$ | 90.00 | 90.00 | 90.00 | 90.00 | 90.00 | 90.00 |
| $SnS_2$ | $a=b$ | 3.64 | 3.68 | 3.62 | 3.67 | 3.63 | 3.60 |
| | $c$ | 5.86 | 5.89 | 5.92 | 6.18 | 6.13 | 6.11 |
| | $\alpha$ | 90.00 | 90.00 | 90.00 | 90.00 | 89.99 | 89.99 |
| | $\beta$ | 90.00 | 90.00 | 90.00 | 90.00 | 90.01 | 90.01 |
| | $\gamma$ | 120.00 | 120.00 | 120.00 | 120.00 | 119.98 | 119.95 |
| ZnS | $a=b=c$ | 5.40 | 5.37 | 5.33 | 5.38 | 5.37 | 5.34 |
| | $\alpha=\beta=\gamma$ | 90.00 | 90.00 | 90.00 | 90.00 | 90.00 | 90.00 |

## References


[1] G. Sai Gautam, T.P. Senftle, and E.A. Carter, Chem. Mater. **30**, 4543 (2018).

[2] D. Broberg, B. Medasani, N.E.R. Zimmermann, G. Yu, A. Canning, M. Haranczyk, M. Asta, and G. Hautier, Comput. Phys. Commun. **226**, 165 (2018).

[3] C. Freysoldt, B. Grabowski, T. Hickel, J. Neugebauer, G. Kresse, A. Janotti, and C.G. Van de Walle, Rev. Mod. Phys. **86**, 253 (2014).

[4] M. Malitckaya, H.-P. Komsa, V. Havu, and M.J. Puska, Adv. Electron. Mater. **3**, 1600353 (2017).

[5] W. Setyawan and S. Curtarolo, Comput. Mater. Sci. **49**, 299 (2010).

[6] S.P. Ong, W.D. Richards, A. Jain, G. Hautier, M. Kocher, S. Cholia, D. Gunter, V.L. Chevrier, K.A. Persson, and G. Ceder, Comput. Mater. Sci. **68**, 314 (2013).

[7] O. Kubaschewski and C.B. Alcock, *Metallurgical Thermochemistry*, 5th ed. (Pergamon Press, 1959).

[8] I. Barin, *Thermochemical Data of Pure Substances* (Wiley, 1995).

[9] D.D. Wagman, W.H. Evans, V.B. Parker, R.H. Schumm, I. Halow, S.M. Bailey, K.L. Churney, and R.L. Nuttall, *Erratum: The NBS Tables of Chemical Thermodynamic Properties. Selected Values for Inorganic and C1 and C2 Organic Substances in SI Units [J. Phys. Chem. Ref. Data 11, Suppl. 2 (1982)]* (American Chemical Society, Washington, DC, 1989).

[10] I. Hurtado, D. Neuschütz, and P. Franke, editors , *Thermodynamic Properties of Inorganic Substances* (Springer, Berlin, 1973).

[11] O. Madelung, U. Rössler, and M. Schulz, editors , *Non-Tetrahedrally Bonded Elements and Binary Compounds I* (Springer-Verlag, Berlin/Heidelberg, 1998).

[12] G. Kim, S. V. Meschel, P. Nash, and W. Chen, Sci. Data **4**, 170162 (2017).

[13] B. Brunetti, V. Piacente, and P. Scardala, J. Alloys Compd. **206**, 113 (1994).

[14] A. Jain, S.P. Ong, G. Hautier, W. Chen, W.D. Richards, S. Dacek, S. Cholia, D. Gunter, D. Skinner, G. Ceder, and K.A. Persson, APL Mater. **1**, 011002 (2013).

[15] P. Villars and K. Cenzual, editors , Https://Materials.Springer.Com/ (2019).